iScience

CellPress
OPEN ACCESS

Article

Biosynthesis of highly branched gold nanoparticles through structural engineering of fatty acids

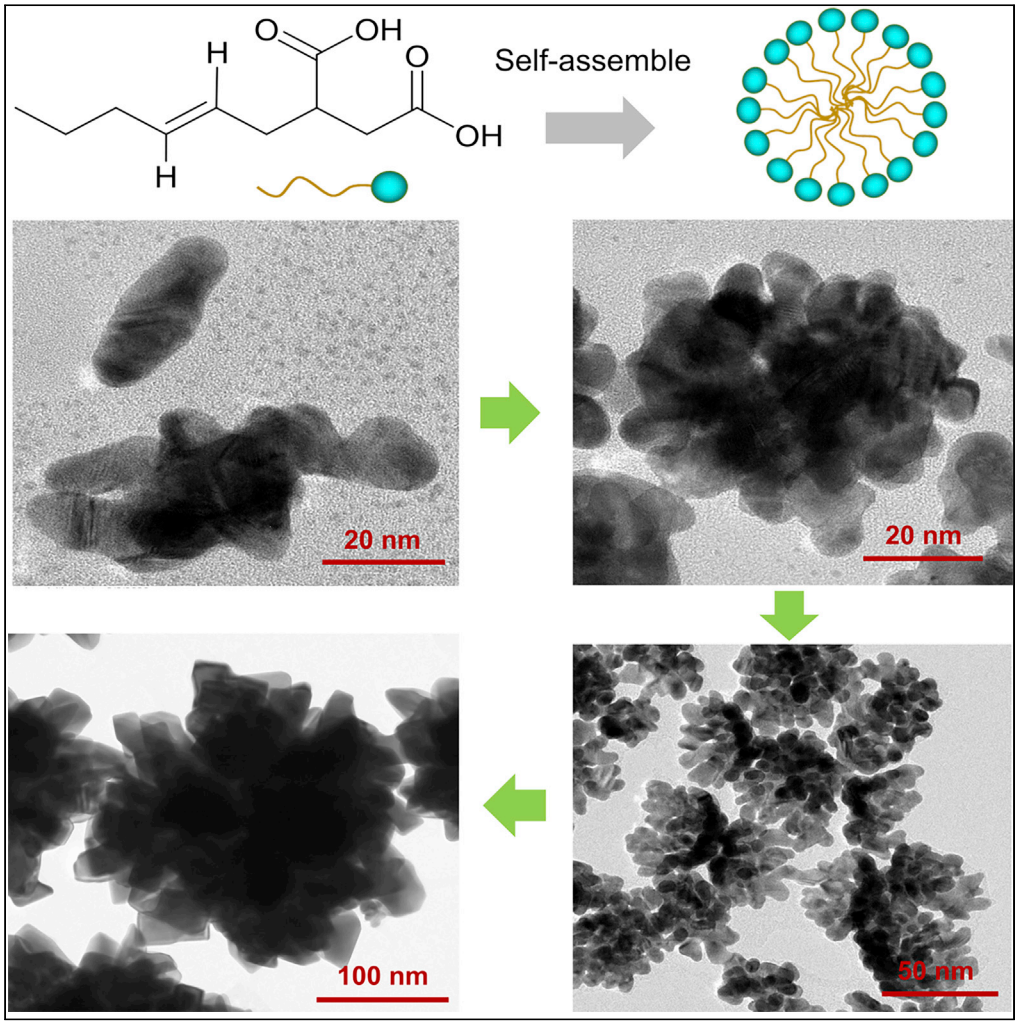

Youfeng Yue, Yoshiko Yokota, Takayuki Uchihashi

yue-yf@aist.go.jp

Highlights

A fatty-acid-directed synthesis of highly branched gold nanoparticle is demonstrated

It is able to control morphologies of nanoparticles from spherical to branched shape

High-speed atomic force microscopy supplies *in situ* observation of particle growth

A general reaction mechanism of nanoparticle formation from fatty acids is proposed

Yue et al., iScience *26*, 105864
January 20, 2023
https://doi.org/10.1016/j.isci.2022.105864

iScience

CellPress
OPEN ACCESS

Article

Biosynthesis of highly branched gold nanoparticles through structural engineering of fatty acids

Youfeng Yue,[1,2,4,*] Yoshiko Yokota,[1] and Takayuki Uchihashi[3]

SUMMARY

Biomimetic approaches have been used to develop inorganic nanomaterials with complex morphologies and functions. Fatty acids are among the most important and decomposable biomolecules in nature. However, the controlled synthesis of branched gold nanoparticles using these biomolecules has not been reported. Herein, we demonstrate a strategy to produce highly branched gold nanoparticles through structural engineering of fatty acids. Furthermore, we developed a method for tailoring fatty acid molecules by altering their aliphatic chains to facilitate the morphological evolution of gold nanoparticles from spherical to branched shape. It is found that the growth of the nanoparticles is sensitive to characteristics of fatty acids, such as saturation degrees. The growth of the nanoparticle is visualized by high-speed atomic force microscopy. The reaction mechanisms and growth processes of branched gold nanoparticles are proposed. This work may serve as a cornerstone to the design in a biomimetic fashion for the controllable synthesis of metallic nanomaterials.

INTRODUCTION

Specific biomaterials/biomolecules produce precise nanostructured inorganic materials with complex morphologies. For example, many single-celled organisms, such as bacteria and algae, can produce inorganic materials either intracellularly or extracellularly.[1–3] Additionally, specific biomolecules that form structural macromolecules, such as lipids, proteins, or peptides, are multifunctional reagents used for the synthesis of biocompatible metal nanoparticles under mild and green conditions.[4] The resulting nanoparticles have a well-defined shape and size and exhibit orientational (e.g., crystalline) symmetry. These structural features are species specific originating from the organic macromolecules that regulate particle growth.

Organic macromolecules play a key role in the formation of inorganic materials during biological evolution (biomineralization), for example, amelogenin formation in human enamel and lustrin formation in abalone nacre.[3] The impact of proteins in mineral forms was studied during *in vitro* biomineralization in these cases.[5] Moreover, the organic macromolecules present in hard biological tissues may affect, independently or in concert, the assembly of hard tissue by regulating mineral synthesis. The combination of inorganic compounds and biological macromolecules in tissues leads to phase compatibility, resulting in excellent biological functions and high impact resistant mechanical properties.

Various biomimetic methods that mimic the natural processes have been developed to create new inorganic materials. Beveridge et al. used *Bacillus subtilis* 168 to synthesize gold nanoparticles on cell walls as early as 1980. They used functional-group-specific modification methods to determine that the carboxyl groups on the cell wall provide the major site of gold nanoparticle deposition.[6] Furthermore, the cell walls in some plants are responsible for regulating crystal nucleation, growth kinetics, phase, and morphology, resulting in biominerals with versatile functions.

The biomimetic approaches for inorganic mineral synthesis are easy, efficient, economical, and eco-friendly. However, the design rules for creating functional biomolecules that aid in the synthesis of metallic nanomaterials with predictable complex morphologies are not well understood. Biomolecules may act as nucleation triggers, growth modifiers, compartments, or scaffolds during mineral formation.[7] Biomolecules may also provide enzymatic effects or act as templates that provide stereochemistry and physisorption for inorganic material formation.[8,9]

[1]Research Institute for Advanced Electronics and Photonics, National Institute of Advanced Industrial Science and Technology (AIST), Tsukuba 305-8565, Japan

[2]Precursory Research for Embryonic Science and Technology (PRESTO), Japan Science and Technology Agency (JST), Kawaguchi 332-0012, Japan

[3]Department of Physics, Nagoya University, Furo-cho, Chikusa-ku, Nagoya 464–8602, Japan

[4]Lead contact

*Correspondence: yue-yf@aist.go.jp

https://doi.org/10.1016/j.isci.2022.105864

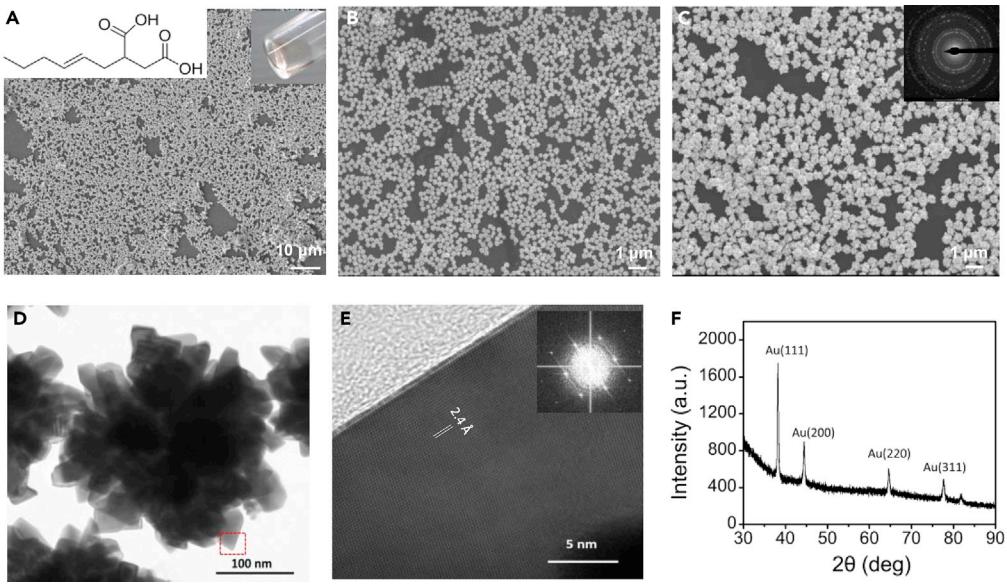

Figure 1. Fatty acids induced formation of branched gold nanoparticles

(A–F) SEM images of the highly branched gold nanoparticles in different scales. These nanoparticles were synthesized in aqueous solution within 30 s (D-F) TEM image, HR-TEM image, and XRD spectrum of the branched nanoparticles. See also Figure S1.

Fatty acids are one of the most important and decomposable biomolecules in nature. They are a major component of lipids (up to 70 wt %) in species, such as microalgae.[10] They are also important dietary sources of fuel for animals and important structural components for cells. Moreover, they cross the cell membranes using specific transport proteins and break down in the cytosol in prokaryotes through beta-oxidation.[11] However, the controlled synthesis of branched metallic nanoparticles using such widely existed biomolecules has not been reported. Unlike protein- and peptide-directed syntheses, there have been long time reports on the controlled synthesis of branched gold nanoparticles.[12] It is the first time to report that fatty acids have significant advantages over these biomolecules from a simple molecule design to achieve a powerful seedless synthesis of branched gold nanoparticles.

Herein, we demonstrate a strategy to regulate the synthesis of highly branched gold nanoparticles in a fast one-step process through fatty acid engineering. Moreover, we developed an efficient method for tailoring fatty acid molecules by altering their aliphatic chains to facilitate the morphological evolution of gold nanoparticles from spherical to branched shape. The length of aliphatic chains, saturation degrees, and number of carboxylic groups in fatty acids are found to be main factors affecting the growth of nanoparticles. The growth of a nanoparticle was visualized by *in situ* high-speed atomic force microscopy (HS-AFM). The mechanisms underlying the reactions of fatty acids and growth process of the derived gold nanoparticles are proposed. This research may provide valuable insights into the design of biomimetic way for the controllable synthesis of metallic nanomaterials.

RESULTS AND DISCUSSION

Fatty-acid-directed synthesis of highly branched gold nanoparticles

Generally, the fatty acids consist of a long alkyl chain of carbon atoms with hydrogen atoms along the length of the chain and carboxyl groups at the head. The carboxylic groups can be anchor groups to bind to metal crystals, fulfilling the important stereochemical requirements.[13,14] Although the binding nature of carboxylic group to gold is not completely understood, it is believed that ionic and coordination interaction are responsible for the binding.[15] The resulted gold metal nanoparticles with complex morphologies may exhibit unique optical, electronic, catalytic, plasmonic, and photothermal properties which have potential applications in biology, medicine, and industry.[14,16,17]

We designed and synthesized different types of fatty acids for producing gold nanoparticles with different lengths of alkyl chains (increased from 4 to 8 carbons), saturation degrees, and numbers of carboxylic

groups (Figure 1, Figure S1). For detail, the fatty acids were dissolved in water at a concentration of ~1.0 wt % under heating, and the gold ions were introduced into the aqueous solution for a typical synthesis procedure. The solution changed color due to surface plasmonic resonance, indicating the formation of gold nanomaterials after mixing the solution for tens of seconds. Interestingly, the fatty acid (C6) with six-carbon alkyl chains produced large amounts of branched nanoparticles observed from scanning electron microscopy (SEM) (Figures 1A–1C).

The selected area electron diffraction pattern of these branched nanoparticles (Figure 1C, inset) consists of a combination of diffraction spots and a ring structure, indicating that the entire particle is nanocrystalline in nature. High-resolution transmission electron microscopy (HR-TEM) images of the branched nanoparticles demonstrate the atomic arrangement and morphology of the gold nanoparticles (Figures 1D and 1E). Moreover, a d-spacing of 2.4 Å was observed in the branched regions with high crystallinity, corresponding to the face-centered cubic (fcc) Au (111) facet Figure 1E).

Five typical diffraction peaks were observed for the nanoparticles at 38.3°, 44.5°, 64.7°, 77.7°, and 81.9° in the 2θ range of 30°–90°, corresponding to the {111}, {200}, {220}, {311}, and {222} reflections of the fcc phase of the gold nanoparticles (Figure 1F). The intensity ratio of {200}:{111} diffraction is 0.50 for the branched nanoparticles. This is approximately equal to the 0.52 intensity ratio of the standard Au diffraction (JCPDS, card No. 04-0784), indicating the synthesized branched nanoparticles were of pure crystalline nature.

Fatty acid (C6) can trigger a magic growth of large quantities of uniquely shaped nanoparticles in a superfast but simple way without any additional energy or separation procedures (e.g., centrifuge). The nanoparticles self-assemble at the interface of water and ethyl acetate after adding ethyl acetate to the solution after synthesis. SEM data further demonstrates that C6 can induce the formation of highly branched-shaped nanoparticles over a tunable range of sizes. For example, the average particle diameters increase gradually from ~289 to ~582 nm with reaction time (Figure S2). The particle size distribution was also analyzed by Zetasizer Nano ZS (Malvern Instruments, UK) from 0.6 to 1000 nm at 25°C. Zetasizer reveals that average size of gold nanoparticles is about 119.0 nm, when the reaction time is further decreased to 5 s (Figure S3).

We also performed energy dispersive X-ray spectroscopy (EDX) spectroscopy in conjunction with TEM to determine the elemental content of the branched nanoparticles. Elements C and O are observed in addition to Au, demonstrating that the organic molecules are coated on the nanoparticles (Figure S4). These organic molecules (from fatty acid) aid in forming intricate inorganic architectures during nucleation, growth, morphology, and crystallization. The fatty acids coating on the nanoparticles were further characterized by EDX mapping and high-resolution TEM, which indicate that the organic coating is about 5 nm (Figure S5). The attached branched regions are single-crystalline particles with excellent lattice patterns, and the whole particle is a polycrystalline consisting of many crystalline parts that are oriented with respect to each other (Figures 1C and 1F).

The optical absorption spectrum of these branched nanoparticles dispersed in water was studied, and the bandgap energy was determined using the Tauc relation.[18]

$$\alpha h\nu = A\left(h\nu - E_g\right)^m \quad (1)$$

where α is the absorption coefficient, h is Planck's constant, ν is the photon's frequency, A is the optical constant, E_g is the bandgap energy, and m is an index which assumes the values ½, 3/2, 2, and 3 depending on the nature of electronic transition. The bandgap energy estimated using Tauc plot (Equation 1) was found to be 4.65 eV (Figure S6), which is close to values reported from other biosynthesized gold nanoparticles.[19]

Compared to other protocols, this biosynthesis has some advantages (Table S1). First, the growth process uses one compound, and can be finished within tens of seconds under a mild heating. Second, the reproducibility is better than other methods due to the simple one-step mixing without stirring. Third, it can reach a high yield of branched nanoparticles with uniform sizes, which is higher than the reported methods that usually need a purification process. To date, the reported methods for synthesizing branched gold nanoparticles are limited to the synthesis of small-sized particles with small branching depths, whereas this biosynthesis method can be used to synthesize highly branched nanoparticles of various sizes even up to 500 nm.

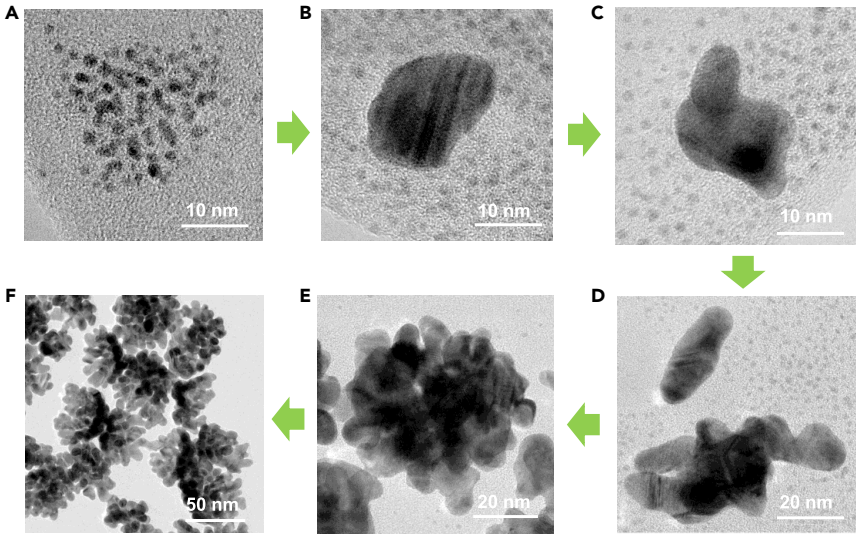

Figure 2. HR-TEM images reveal the early-stage formation of branched gold nanoparticles triggered by C6 fatty acid

(A) Formation of the small nanoparticles with diameter of 1–2 nm.

(B) Small nanoparticles grow and merge into a plate-like particle.

(C) Distorted nanoplate is formed.

(D–F) Distorted nanoplates growth into nanoclusters (E, F) with diameters of 30–50 nm. The images of the nanoclusters indicate that they are highly branched. See also Figure S7.

Early stage of the branched nanoparticle formation

Many branched nanoparticles were observed in the SEM images, captured within tens of seconds of mixing the sample under a mild heating. Thus, the early stages of intermediate formation occur within seconds of mixing the sample. The early stages of the structure formation of gold nanoparticles are characterized using TEM (Figure 2). The gold ions instantly bind to the head of C6 organics and nucleate into small gold nanoparticles with diameters of approximately 1–2 nm when the gold ions are added to the C6 aqueous solution (Figure 2A). These small nanoparticles have irregular sizes and consist of hundreds of atoms (for example, a gold nanoparticle with a diameter of 1.5 nm consists of 840 atoms). Subsequently, the nanoparticles grow and merge into a nanoplate-like structure with a diameter of 10 nm (Figure 2B). The deposition of nanocrystals in the C6 organic molecules involves controlled nucleation at the interfaces between the crystals and organic molecules. Moreover, the remaining deposited nanoparticles result in the continuous growth of distorted nanoplates (Figure 2C). The distorted nanoplates attach together (Figure 2D) and grow into small nanoclusters approximately 30–50 nm in size as well as some twin-like structures (Figures 2E, 2F and S7). These specific nanoclusters with size smaller than 100 nm are act as intermediates for the fast growth of large-sized highly branched particles, which can reach sizes of several hundred nm varied with the reaction time.

The C6 consists heads of two carboxylic groups that act as binders for the continuous growth of nanoplates and induced an attachment of distorted nanoplates into a cluster. Moreover, the 6-carbon length of alkyl chain with a balance of hydrophobicity is critical for the formation of highly branched nanoparticles. The two carboxylic groups are separated by two carbon atoms, and the balance of hydrophobicity from the long alkyl chains provides an ideal binding affinity and high capacity to accept the aqueous gold ions for controlling the nucleation. An unbalanced hydrophobicity or a strong binding affinity may inhibit the nucleation because strong binding removes the aqueous gold ions from solution, rendering them unreactive.[13] Moreover, a high capacity is necessary to localize a sufficient number of gold ions at the matrix surface to exceed the critical particle growth threshold. Fatty acid C6 achieves a satisfactory balance of hydrophobicity and binding affinity, resulting in the formation of a unique highly branched nanostructure. However, a change in the length of alkyl chains (either increase to 8 or decrease to 4 carbons) fails to achieve any highly branched nanoparticle structures. Additionally, thermogravimetric analysis (TGA) and differential scanning calorimetry (DSC) analysis were also used to measure the thermal characteristic of the fatty acid C6. The TGA measurement performed under nitrogen gas flow showed that the samples

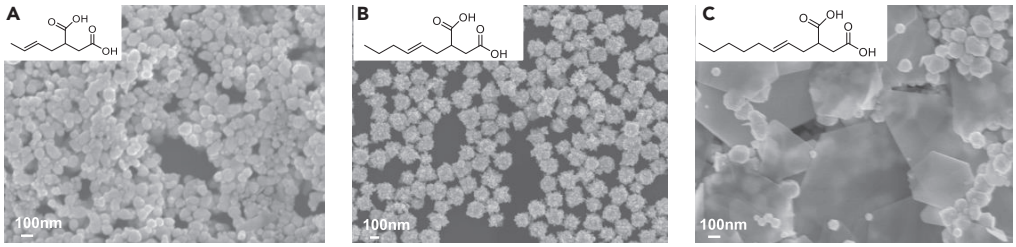

Figure 3. Variations in the morphology of the gold nanoparticles produced using fatty acids with different length of alkyl chains

(A) Fatty acids with a short alkyl chain (four carbons) form nanoparticles with irregular shapes.

(B) Fatty acids with an alkyl chain of six carbons form highly branched nanoparticles.

(C) Fatty acids with a long alkyl chain of eight carbons form nanoplates mixed with nanoparticles.

undergo a single mass-loss process. The DSC signal exhibited an endothermic peak at about 65.7°, indicating the melting temperature of C6 was 65.7° (Figure S8).

Structural engineering of fatty acid for controllable synthesis of gold nanoparticles

Length of the alkyl chains in fatty acids

Since such superfast, high-yield, seedless synthesis process has not been reported in the literature, it is important to explore the deep in the molecular structures and to reveal the design rules for fatty-acid-directed metal nanoparticle synthesis. We designed numerous fatty acids and analyzed the particle formation process corresponding to each fatty acid. It is found that the length of an alkyl chain has an impact on the morphology of resultant nanoparticles. Fatty acids with different aliphatic chains resulted in corresponding nanoparticles (Figure 3). Fatty acids with a short alkyl chain (four carbons) form nanoparticles with irregular shapes (Figure 3A), fatty acids with an alkyl chain of six carbons form highly branched nanoparticles (Figure 3B), and fatty acids with a long alkyl chain of eight carbons form nanoplates mixed with nanoparticles (Figure 3C). This result demonstrates that the length of fatty acids with a balanced of hydrophobicity is crucial for controlling the morphology of gold nanoparticles.

Function of saturation of the fatty acids

The above used fatty acids all contain unsaturated alkyl chains (C=C double bond). A fatty acid is a carboxylic acid with a saturated (C-C single bond) or unsaturated (C=C double bond) alkyl chain existing as a part of the lipid bilayer or triglycerides in lipid droplets. Double bonds (C=C) in fatty acids alter the fluidity of cell membranes and the melting temperature of fat because *cis* isomers restrict the close packing of *trans* isomers.[20]

We further found for the first time that the saturation/unsaturation level in a fatty acid has a significant impact on their reduction ability toward synthesis of gold nanoparticles. For example, we synthesized two fatty acids (C4): one with a double bond (unsaturated) and the other without any double bond (saturated) (Figure S9).

The control experiments demonstrated that the unsaturated fatty acid rapidly reduced the gold ions into gold nanoparticles, with a color change owing to surface plasmon resonance absorption within a few seconds (Figure S9). However, the saturated one has no ability to reduce the gold ions even with a high heating temperature (56°C) for more than 4 h. No nanoparticles were observed in the SEM images for the saturated C4 fatty acid further indicating that the saturated C4 fatty acid could not effectively reduce Au^{3+} to Au^{0}. This observation is important for the future design of specific fatty acids for the control synthesis of metallic nanoparticles.

Number of carboxylic groups of the fatty acids

We also performed controlled experiments using fatty acids with different numbers of carboxylic groups to analyze the impact of the number of carboxylic groups on the formation of nanoparticles.

The experiments demonstrated that all the tested fatty acids (either with one or two carboxylic groups) could produce gold nanoparticles (Figure S10). However, the fatty acid with two carboxylic groups

exhibited highest efficiency and rapid formation of nanoparticles than the ones with only one carboxylic group. The fatty acids with one carboxylic group produce nanoparticles in a slow way; they need several days to produce nanoparticles at room temperature, indicating the producing efficiency is thousands of times lower than the one with two carboxylic groups at the same condition in terms of reaction time. Moreover, some fatty acids (for example, 3-heptenoic acid) that exist in an oil state at room temperature (25°C) are immiscible with water because of phase separation. However, they can also produce nanoparticles in the oil phase with a change in color from transparent to gray (Figure S10).

Among all the tested fatty acids, only C6 with two carboxylic groups produced nanoparticles with a unique branched structure. These results further demonstrate the importance of the chemical structure engineering of fatty acids in the synthesis of metallic nanoparticles.

Observation of the structural macromolecules

As we all known, natural biomolecules usually exist as structural macromolecules (lipids, proteins, or polysaccharides) that control the growth kinetics of inorganic compounds during biomineralization. The organic macromolecules play a key role in initiating the formation (nucleation) of inorganic solids (for example, calcium phosphate crystals of bones). These natural processes inspire us to think about why the C6 molecules can synthesize branched nanoparticles. The process may also arise not from the action of individual molecules, but from their macromolecules. To explore this, we then studied the macromolecular structure of C6 in an aqueous solution to further uncovering the mechanisms for fatty-acid-directed synthesis of nanoparticles.

However, detecting the nanoscale organic macromolecule structures in water is difficult. The water solution of C6 is transparent and close to the state of water. We first used freeze-fracture TEM to observe the macromolecular structure. The aqueous solution with a concentration of 1.0 wt % C6 fatty acid was dropped in the specimen carrier and frozen in liquid nitrogen. The frozen samples were fractured at −120°C in a vacuum chamber. Subsequently, the samples were coated with platinum, followed by carbon, and their TEM images were recorded using a CDD camera. As shown in Figure 4A, there is a spherical (diameter: 80 nm) structure, probably from a macromolecular aggregation of C6.

The view scale from TEM images is limited, which is in contrast with the large number of nanoparticles collected from the solution. Thus, HS-AFM was used to capture images because it was a powerful and advanced technology for observing the dynamic organic macromolecular structures in water.[21,22]

The HS-AFM image showed spherical particles with a diameter of around 50 nm on mica surface, indicating that C6 organics disperses in water as an aggregate (Figure 4B). When the force applied from the probe tip was increased during imaging, the size of the sphere decreased by about 10 nm, suggesting that the C6 macromolecular aggregate is mechanically soft (Figure 4C, Video S1). Furthermore, when gold ions were added to the solution in a 0.4 wt % C6 fatty acid solution during the HS-AFM imaging of mica surface, it is exciting to visualize that a gold particle appeared onto the mica surface and growth with time (Figure 4D, Video S2). Although the early stage of the particle formation is difficult to observe, the growth of a nanoparticle with increasing in islands (branched region) has been directly visualized *in situ* by HS-AFM (Figures 4D and S11). The high spatiotemporal resolution enabled us to observe the structure of organic macromolecules (without gold ions) in water and the rapid growth of gold particles under the coexistence of gold ions and C6 fatty acids. These existing organic macromolecules have nanoscale spherical shapes, interacted and regulated with the metal ions, causing enzymatic reactions and acting as templates. They are experimentally confirmed to be crucially important for the large-scale and high-efficiency-producing gold nanoparticles with uniform size and unique crystal morphology (Figure S12).

Reaction mechanisms of fatty acids in synthesis of nanoparticles

Uncovering the reaction mechanisms for these fatty-acid-directed syntheses is also important. We try to explore the general reduction mechanisms for the production of gold nanoparticles using these fatty acids.

We characterized the chemical structures of fatty acids during the reaction using proton nuclear magnetic resonance (^{1}H NMR) spectroscopy. As shown in Figure 5A, changes occur in the chemical structure of the fatty acid (C6) during nanoparticle synthesis. The single peak at a chemical shift of 0.88 ppm before the reaction (t = 0) represents the protons from the terminal methyl group, and the peaks at 5.50 and 5.34 ppm represent the

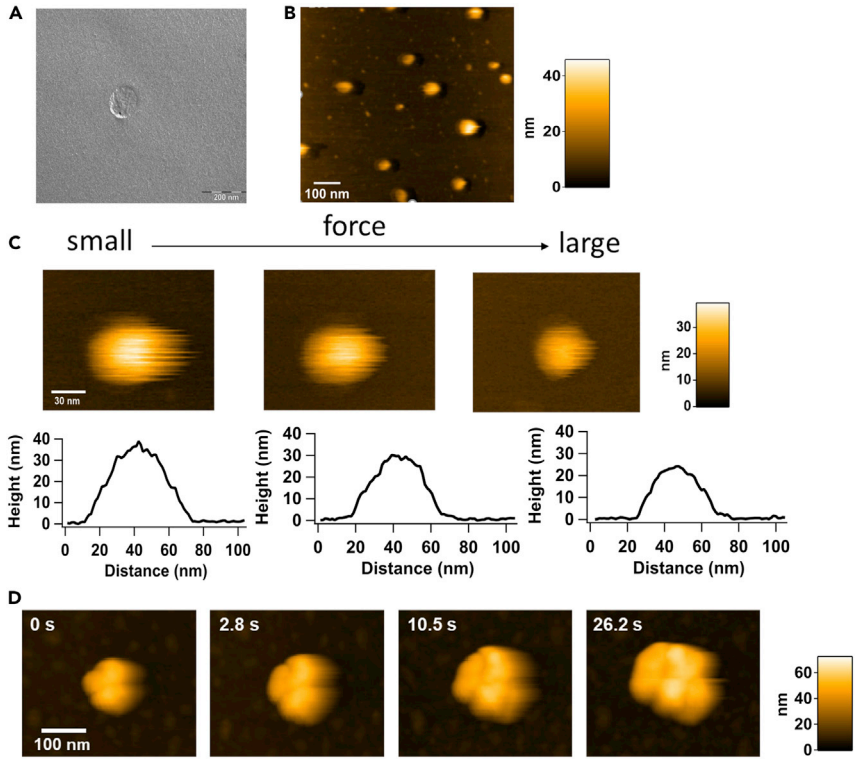

Figure 4. Fatty acids form macromolecues and growth of branched gold nanoparticles observed under HS-AFM

(A and B) Freeze-fracture TEM and (B) HS-AFM to observe the macromolecular structure of C6 in the aqueous solution.

(C) Decrease in the height of the C6 macromolecule with increasing loading force during HS-AFM imaging.

(D) Growth of the gold particle in a solution including C6 fatty acids and gold ions. A movie showing *in-situ* observing macromolecular structure change of C6 fatty acids in water, and a movie showing the growth of a single gold nanoparticle in water by using HS-AFM can be seen in the Videos S1 and S2.

two protons near the double bonds of fatty acid. The integrals of the double bond protons near 5.50 ppm decrease gradually from 1 to 0.6, corresponding to the increase in reaction time when all the integrals of the terminal methyl are fixed at three. This indicates that some of the double bonds in the fatty acid disappear during the nanoparticle formation. Moreover, the new peaks appearing at 5.88 and 1.01 ppm further represent the changes in the chemical structure of fatty acids during nanoparticle formation. Other fatty acids with long alkyl chains (C8 and C12) exhibited similar ^{1}H NMR spectral changes during the gold nanoparticle formation reactions (Figure S13).

Based on this, we proposed a general reduction mechanism for fatty-acid-directed synthesis (Figures 5B and 5C). As shown in Figure 5A, the appearance of protons at 1.01 ppm indicates the shortening of carbon skeleton in the fatty acids because of decarboxylation during the reduction reaction. The two carboxyl groups in the fatty acid are separated by two carbons that are prone to decarboxylation accompanied by a carbon skeleton rearrangement.[23] The resultant compound forms a conjugated structure and reacts with water to form an intermediate hydroxy compound with a functional group (–OH) to reduce the gold ions to gold nanoparticles. Subsequently, the hydroxy compound is oxidized into acetoacetate and degraded (alkane degradation) due to the loss of acetic acid. This results in the protons near the double bonds and the terminal methyl group shifting to high ppm values (to 5.88 and 1.01 ppm, respectively). The continuous loss of acetic acid shortens the carbon skeleton, consumes the double bond, and decomposes the fatty acids. Thus, the integral of protons near the double bond decreases as shown in the ^{1}H NMR spectrum. The proposed procedures are very similar to that of the fatty acid degradation by bacteria in nature.[23,24] The fatty acids sacrifice themselves to produce large numbers of nanoparticles. After reaction, most of the C6 fatty acids degraded into small molecules (such as propionic acid), which are easy to be dissolved in water. Some byproducts or the residual fatty acids become the dispersion agents for stabilizing the nanoparticles.

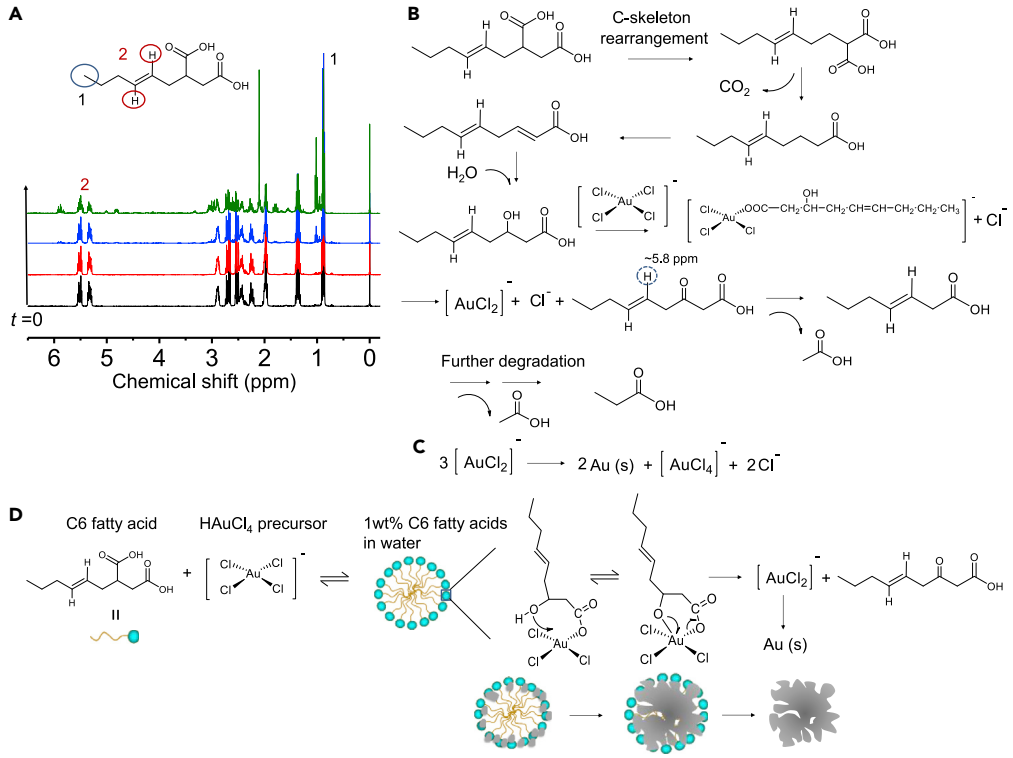

Figure 5. The proposed reaction mechanisms of nanoparticles formation between fatty acids and precursor

(A) ^{1}H NMR spectrum change of fatty acid before and after the reduction of gold ions into gold nanoparticles with time. (B–D) The proposed reaction mechanisms for nanoparticle formation.

Electrospray ionization mass spectrometry was used to characterize the organic compounds before and after formation of gold nanoparticles. The mass spectrum changed significantly after nanoparticles formation, indicating the presence of byproducts after synthesis of gold nanoparticles (Figure S14). However, its isolation from the reaction mixture was found to be complex due to its decomposition to form many byproducts, such as acetoacetate (Figure 5B). The change from intermediate hydroxy compound to acetoacetate was also postulated in previous studies and was generally accepted for the formation of gold nanoparticles.[25–27]

The fatty acid is expected to equatorially coordinate and replace a planar Cl^{-} ligand to form the corresponding complex $[AuCl_3(C_9H_{15}O_3)]^{-}$ (Figures 5B and 5D). Deprotonation of the alcohol group and coordination of the alcohol oxygen with Au(III) gives a coordinated intermediate complex (Figure 5D), which will be further disintegrated into Au (I) and acetoacetate products.[27] The resulting Au(I) species can finally form Au (0) atoms (Figures 5C and 5D).[28] In the case of C6 fatty acid, they form spherical-shaped biomacromolecules at a specific concentration (~1 wt %) in water (Figure 5D). The reactions with gold ions are initiated on the surface of the spherical biomacromolecules because the functional carboxylic groups are hydrophilic. The reactions occur at different locations of the biomacromolecule surface, which play a critical role in the formation of branched gold nanoparticles (Figure 5D).

Conclusions

We demonstrate a strategy to regulate the synthesis of highly branched gold nanoparticles in a fast one-step process through fatty acid engineering. Furthermore, we develop an efficient method for tailoring fatty acid molecules by altering their aliphatic chains to facilitate the morphological evolution of gold nanoparticles from spherical to branched shape. The length, saturation of aliphatic chains, and number of carboxylic groups in the fatty acids are found to be the main factors that affect the growth of gold nanoparticles. The macromolecular aggregation structure of C6 fatty acid and the rapid growth of branched nanoparticles are successfully observed *in situ* by HS-AFM. Furthermore, we explore the mechanisms of the reduction reactions of fatty acids and growth mechanisms of the gold nanoparticles. This work provides valuable insights into the design of fatty acids for the controllable biosynthesis of branched gold nanoparticles.

Limitations of the study

This work provides a systematic experimental technique to produce highly branched gold nanoparticles by manipulation of the structure of fatty acids. The mechanisms underlying the reactions of fatty acids and growth process of the derived gold nanoparticles are proposed. However, strong experimental evidence for all the reaction mechanisms, processes of nanoparticle formation, and their potential applications in different fields need to be further explored.

STAR★METHODS

Detailed methods are provided in the online version of this paper and include the following:

- KEY RESOURCES TABLE
- RESOURCE AVAILABILITY
  - Lead contact
  - Materials availability
  - Data and code availability
- EXPERIMENTAL MODEL AND SUBJECT DETAILS
- METHOD DETAILS
  - Fatty acid synthesis
  - Branched gold nanoparticle synthesis
  - HS-AFM observation
  - Characterizations
- QUANTIFICATION AND STATISTICAL ANALYSIS

SUPPLEMENTAL INFORMATION

Supplemental information can be found online at https://doi.org/10.1016/j.isci.2022.105864.

ACKNOWLEDGMENTS

This research is partially supported by the Japan Society for the Promotion of Science (JSPS) KAKENHI (Grant Nos. JP20H04683, JP20H05237) and by Japan Science and Technology Agency (JST), Precursory Research for Embryonic Science and Technology (PRESTO), Grant No. JPMJPR209A.

AUTHOR CONTRIBUTIONS

Y.Yue designed the project. Y.Yue prepared the nanoparticles. Y.Yue, Y.Yokoda, and T.U. performed the characterization experiments. Y.Yue and T.U. wrote the manuscript. All authors discussed the results and commented on the manuscript.

DECLARATION OF INTERESTS

The authors declare no competing interest.

INCLUSION AND DIVERSITY

We support inclusive, diverse, and equitable conduct of research.

Received: September 26, 2022
Revised: November 28, 2022
Accepted: December 20, 2022
Published: January 20, 2023

REFERENCES

1. Santhosh, P.B., Genova, J., and Chamati, H. (2022). Green synthesis of gold nanoparticles: an eco-friendly approach. Chemistry (Easton) *4*, 345–369. https://doi.org/10.3390/chemistry4020026.

2. Simkiss, K., and Wilbur, K.M. (2012). Biomineralization (Elsevier), pp. 22–30.

3. Sarikaya, M. (1999). Biomimetics: materials fabrication through biology. Proc. Natl. Acad. Sci. USA *96*, 14183–14185. https://doi.org/10.1073/pnas.96.25.1418.

4. Tan, Y.N., Lee, J.Y., and Wang, D.I.C. (2010). Uncovering the design rules for peptide synthesis of metal nanoparticles. J. Am. Chem. Soc. *132*, 5677–5686. https://doi.org/10.1021/ja907454f.

5. Falini, G., Albeck, S., Weiner, S., and Addadi, L. (1996). Control of aragonite or calcite polymorphism by mollusk shell macromolecules. Science *271*, 67–69. https://doi.org/10.1126/science.271.5245.6.

6. Beveridge, T.J., and Murray, R.G. (1980). Sites of metal deposition in the cell wall of Bacillus subtilis. J. Bacteriol. *141*, 876–887. https://doi.org/10.1128/jb.141.2.876-887.1980.

7. Addadi, L., and Weiner, S. (1992). Control and design principles in biological mineralization. Angew. Chem. Int. Ed. Engl. *31*, 153–169. https://doi.org/10.1002/anie.199201531.

8. Addadi, L., and Weiner, S. (1985). Interactions between acidic proteins and crystals: stereochemical requirements in biomineralization. Proc. Natl. Acad. Sci. USA *82*, 4110–4114. https://doi.org/10.1073/pnas.82.12.4110.

9. Greenfield, E.M., Wilson, D.C., and Crenshaw, M.A. (1984). Ionotropic nucleation of calcium carbonate by molluscan matrix. Am. Zool. *24*, 925–932. https://doi.org/10.1093/icb/24.4.925.

10. Chen, L., Liu, T., Zhang, W., Chen, X., and Wang, J. (2012). Biodiesel production from algae oil high in free fatty acids by two-step catalytic conversion. Bioresour. Technol. *111*, 208–214. https://doi.org/10.1016/j.biortech.2012.02.033.

11. Houten, S.M., and Wanders, R.J.A. (2010). A general introduction to the biochemistry of mitochondrial fatty acid β-oxidation. J. Inherit. Metab. Dis. *33*, 469–477. https://doi.org/10.1007/s10545-010-9061-2.

12. Yan, F., Liu, L., Walsh, T.R., Gong, Y., El-Khoury, P.Z., Zhang, Y., Zhu, Z., De Yoreo, J.J., Engelhard, M.H., Zhang, X., and Chen, C.L. (2018). Controlled synthesis of highly-branched plasmonic gold nanoparticles through peptoid engineering. Nat. Commun. *9*, 2327–2334. https://doi.org/10.1038/s41467-018-04789-2.

13. Mann, S. (1988). Molecular recognition in biomineralization. Nature *332*, 119–124. https://doi.org/10.1038/332119a0.

14. Yue, Y., and Norikane, Y. (2020). Gold clay from self-assembly of 2D microscale nanosheets. Nat. Commun. *11*, 568–576. https://doi.org/10.1038/s41467-019-14260-5.

15. Paik, W.k., Han, S., Shin, W., and Kim, Y. (2003). Adsorption of carboxylic acids on gold by anodic reaction. Langmuir *19*, 4211–4216. https://doi.org/10.1021/la026836s.

16. Giljohann, D.A., Seferos, D.S., Daniel, W.L., Massich, M.D., Patel, P.C., and Mirkin, C.A. (2010). Gold nanoparticles for biology and medicine. Angew. Chem. Int. Ed. Engl. *49*, 3280–3294. https://doi.org/10.1002/anie.200904359.

17. Elahi, N., Kamali, M., and Baghersad, M.H. (2018). Baghersad MH. Recent biomedical applications of gold nanoparticles: a review. Talanta *184*, 537–556. https://doi.org/10.1016/j.talanta.2018.02.088.

18. Tauc, J., and Menth, A. (1972). States in the gap. J. Non-Cryst. Solids *8–10*, 569–585. https://doi.org/10.1016/0022-3093(72)90194-9.

19. Singh, N., Das, M.K., Ansari, A., Mohanta, D., and Rajamani, P. (2021). Biogenic nanosized gold particles: physico-chemical characterization and its anticancer response against breast cancer. Biotechnol. Rep. *30*, e00612–e00622. https://doi.org/10.1016/j.btre.2021.e00612.

20. Rustan, A.C., and Drevon, C.A. (2001). Fatty Acids: Structures and Properties. *Encycl Life Sci* (John Wiley & Sons), pp. 1–3.

21. Ando, T., Kodera, N., Takai, E., Maruyama, D., Saito, K., and Toda, A. (2001). A high-speed atomic force microscope for studying biological macromolecules. Proc. Natl. Acad. Sci. USA *98*, 12468–12472. https://doi.org/10.1073/pnas.211400898.

22. Konno, H., Watanabe-Nakayama, T., Uchihashi, T., Okuda, M., Zhu, L., Kodera, N., Kikuchi, Y., Ando, T., and Taguchi, H. (2020). Dynamics of oligomer and amyloid fibril formation by yeast prion Sup35 observed by high-speed atomic force microscopy. Proc. Natl. Acad. Sci. USA *117*, 7831–7836. https://doi.org/10.1073/pnas.1916452117.

23. Davidova, I.A., Gieg, L.M., Nanny, M., Kropp, K.G., and Suflita, J.M. (2005). Stable isotopic studies of n-alkane metabolism by a sulfate-reducing bacterial enrichment culture. Appl. Environ. Microbiol. *71*, 8174–8182. https://doi.org/10.1128/AEM.71.12.8174-8182.2005.

24. Wilkes, H., Rabus, R., Fischer, T., Armstroff, A., Behrends, A., and Widdel, F. (2002). Anaerobic degradation of n-hexane in a denitrifying bacterium: further degradation of the initial intermediate (1-methylpentyl) succinate via C-skeleton rearrangement. Arch. Microbiol. *177*, 235–243. https://doi.org/10.1007/s00203-001-0381-3.

25. Munro, C.H., Smith, W.E., Garner, M., Clarkson, J., and White, P.C. (1995). Characterization of the surface of a citrate-reduced colloid optimized for use as a substrate for surface-enhanced resonance Raman scattering. Langmuir *11*, 3712–3720. https://doi.org/10.1021/la00010a021.

26. Xue, C., Métraux, G.S., Millstone, J.E., and Mirkin, C.A. (2008). Mechanistic study of photomediated triangular silver nanoprism growth. J. Am. Chem. Soc. *130*, 8337–8344. https://doi.org/10.1021/ja8005258.

27. Ojea-Jiménez, I., Romero, F.M., Bastús, N.G., and Puntes, V. (2010). Small gold nanoparticles synthesized with sodium citrate and heavy water: insights into the reaction mechanism. J. Phys. Chem. C *114*, 1800–1804. https://doi.org/10.1021/jp9091305.

28. Gammons, C.H., Yu, Y., and Williams-Jones, A. (1997). The disproportionation of gold (I) chloride complexes at 25 to 200 C. Geochem. Cosmochim. Acta *61*, 1971–1983. https://doi.org/10.1016/S0016-7037(97)00060-4.

STAR★METHODS

KEY RESOURCES TABLE

REAGENT or RESOURCE	SOURCE	IDENTIFIER
Chemicals, peptides, and recombinant proteins		
C6 fatty acid anhydride	TCI Co., Japan	CAS: 10500-34-2
C4 fatty acid anhydride	TCI Co., Japan	CAS: 7538-42-3
C8 fatty acid anhydride	TCI Co., Japan	CAS: 42482-06-4
Gold (III) chloride trihydrate	Sigma-Aldrich	CAS: 16961-25-4
Ethyl acetate	Wako Pure Chemical Ind., Ltd.	CAS: 141-78-6
NaOH	Wako Pure Chemical Ind., Ltd.	CAS: 1310-73-2
Acetone	Kishida Chemical Co.,Ltd.	CAS: 67-64-1
Chloroform -D (D, 99.8%) +0.05% V/V TMS	Cambridge Isotope Laboratories Inc.	Product code: DLM-7TB
Distilled water	Merck Millipore	Direct-Q 3UV
Software and alogorithms		
TEM DigitalMicrograph	Gatan Microscopy Suite	https://www.gatan.com/
Origin Pro	Origin Lab	https://www.originlab.com/
Microsoft Powerpoint	Microsoft Office	https://www.office.com/
Chem Draw	PerkinElmer	https://perkinelmerinformatics.com/products/research/chemdraw

RESOURCE AVAILABILITY

Lead contact

Further information and requests for resources should be directed to and will be fulfilled by the lead contact, Youfeng Yue (yue-yf@aist.go.jp).

Materials availability

This study did not generate new unique reagents.

Data and code availability

- All data reported in this paper will be shared by the lead contact upon request.
- This paper does not report original code.
- Any additional information required to reanalyze the data reported in this paper is available from the lead contact upon request.

EXPERIMENTAL MODEL AND SUBJECT DETAILS

Our study does not use experimental models typical in the life sciences.

METHOD DETAILS

Fatty acid synthesis

The C6 fatty acid was synthesized from their anhydride compounds in aqueous NaOH (6M) at ~100°C with strong stirring. The reaction was stopped by adding large amount of water. The pH values of the solution were adjusted to ~2 by adding HCl solution (2M). The compounds were extracted by ethyl acetate and washed with water for more than three times. The pure compounds were recrystallized in acetone.

Branched gold nanoparticle synthesis

The gold (III) chloride trihydrate with a concentration of 2×10^{-2} M was prepared and kept in fridge for use. The C6 fatty acids (50 mg) were dissolved in water (5.0 mL) with a concentration of 1.0 wt %, and then the

prepared gold ions (120 μL) were dropped into the aqueous solution. After mixing for 300 s under a mild heating (~37°C) without any stirring, the solution changed from light yellow to slightly greenish, indicating the formation of branched gold nanoparticles. The growth of the nanoparticles can be stopped by adding ethyl acetate to the mixed solution. With shaking, the nanoparticles were self-assembled in the interface of water and ethyl acetate. When the reaction temperature was increased to 53°C, the synthesis can be finished within tens of seconds.

HS-AFM observation

We used a laboratory-built high-speed AFM. HS-AFM is operated in tapping mode using a small cantilever with a spring of ~0.2 N/m, a resonant frequency of ~700 kHz, and quality factor of ~2 in a solution. To observe the C6 macromolecules, a droplet of 1.2 wt % fatty acid was deposited on a freshly cleaved mica substrate and incubated for 10 min followed by washing with ultra-pure water. HS-AFM imaging was carried out in water. For the observation of gold particles, a solution of gold ions was added while observing the mica substrate in 0.4 wt % fatty acid solution. Immediately after the addition of gold ions into the observation solution, the HS-AFM imaging becomes quite unstable due to the large decrease in light reflection at the cantilever, but after recovery, we observed gold particles adsorbed on the mica surface and monitored the growth of the gold particle. All HS-AFM imaging was carried out at room temperature (25°C).

Characterizations

The chemical structures of the synthesized fatty acids were characterized by the nuclear magnetic resonance (^{1}H NMR) characterization on a Bruker Advance III NMR spectrometer (Switzerland) at a resonance frequency of 400 MHz. SEM images were obtained on a field emission scanning electron microscope JSM-6340F (JEOL, Japan) at an operating voltage of 10 kV. TEM was measured on a Tecnai Osiris (USA), which was equipped with an energy-dispersive spectroscopy detector. X-ray diffraction data were collected on a SmartLab Rigaku-X-ray analytical machine (USA) with Cu Kα (λ = 1.5418 Å). The freeze-fracture TEM images were obtained in a JEOL JEM-1010 electron microscope (JEOL, Tokyo, Japan) operating at 110V. UV-Vis absorption spectra were recorded on a JASCO V-670 using double-beam spectrophotometer. Thermogravimetric analysis (TGA) was carried out with a Seiko TG-DTA 6200-S. The measurement was performed with a temperature increasing speed of 10 °C/min from 25 to 500°C. Differential scanning calorimetry (DSC) measurement was performed on EXSTAR SII DSC6220 with a temperature increasing/decreasing speed of 5 °C/min. The particle size distribution was analyzed by Nanosizer Nano ZS (Malvern Instruments, Worcestershire, UK) from 0.6 to 1000 nm at 25°C, in which the peak position was automatically calculated. The water refractive index (RI) of 1.33 and the water viscosity of 0.8872 cP were employed. The mass spectra were measured on a Bruker micrOTOF II instrument.

QUANTIFICATION AND STATISTICAL ANALYSIS

All the measurements are tested at least three independent experiments. The TEM images were collected and analyzed by Gatan Microscopy Suite. The particle sizes were obtained from SEM by measuring the diameters at 60 points. The particle sizes were also measured from zetasizer instrument twice. Data tabulation, analysis, and plotting were performed in Origin 2019 software.